



Free convective heat transfer and entropy generation characteristics of the nanofluid flow inside a wavy solar power plant

Sumit Kumar Mehta¹ · Pranab Kumar Mondal²

Received: 19 February 2022 / Accepted: 8 July 2022 / Published online: 22 July 2022
© The Author(s), under exclusive licence to Springer-Verlag GmbH Germany, part of Springer Nature 2022

Abstract

We have numerically investigated the natural convective heat transfer and entropy generation characteristic inside a wavy solar power plant filled with MWCNT-Fe₃O₄-water nanofluid using the finite element method. The simulated flow and temperature fields are investigated in terms of streamline contour, isotherm contour, local Nusselt number, average Nusselt number, dimensionless total entropy generation, and dimensionless average total entropy generation by varying the dimensionless amplitude of the wavy wall and nano-particle volume fraction. We reported that the presence of a wavy wall and the addition of nano-particles decreases the strength of recirculation developed in the flow field. Moreover, as seen from the analysis, an increase in the amplitude of the wavy wall and nano-particle volume fraction enhances the average Nusselt number. The entropy generation due to viscous dissipation is dominated for the considered value of the Rayleigh number. In addition, our results show that the increase in wave amplitude and nano-particle volume fraction reduces the average entropy generation. Inferences of this analysis are expected to have far ranging consequences to the optimum design of the solar power plant.

1 Introduction

In recent times, solar energy is one of the most suitable clean energy and an excellent alternative for conventional energy (Farshad et al. 2019; Ebrahimpour et al. 2021; Kumar et al. 2021a, b). For most solar power plants, the heat transfer enhancement should be maximum in order to achieve higher exergetic efficiency (Huang and Hsu 2019; Krishna et al. 2019; Selimefendigil and Oztop 2019; Sureshkumar Raju et al. 2019; Alblawi et al. 2020). Therefore, researchers used many active and passive techniques to improve the heat transfer rate in the past decades. The use of wavy wall, nanofluids, porous media are some common examples of passive techniques, while the application of magnetic and electric field are the examples of active technique (Huang and Hsu 2019;

Krishna et al. 2019; Selimefendigil and Oztop 2019; Sureshkumar Raju et al. 2019; Alblawi et al. 2020; Shyam et al. 2020, 2021; Mondal and Wongwises 2020; Tyagi et al. 2020; Kumar and Mondal 2022).

It may be mentioned here that for solar plants, natural convection is a suitable means of heat transfer (Ma et al. 2020). A number of investigations have been reported to improve the natural convective heat transfer rate by using active and passive techniques. Recently, hybrid nanofluid has been used for better heat transfer rate instead of a single component of nanofluid. The hybrid nanofluid gives improved thermal characteristics. Some of the examples of hybrid nanofluids are Ag-MgO-water nanofluid (Ghalambaz et al. 2020; Goudarzi et al. 2020), Al₂O₃-Cu-water nanofluid (Mansour et al. 2018; Tayebi and Chamkha 2021; Roy 2022), MWCNT (multi-walled carbon nanotubes)-Fe₃O₄-water nanofluid (Sundar et al. 2014; Brusly Solomon et al. 2017a, b; Izadi et al. 2018, 2019; Sajjadi et al. 2019; Mourad et al. 2021). Goudarzi et al. (2020) investigated the effect of thermophoresis and Brownian motion of Ag-MgO-Water hybrid nanofluid on the natural convective transport of heat. It is found that the thermophoresis migration causes more accumulation of nano-particle near the cold wall. Ghalambaz et al. (2020) reported the effect of Ag-MgO-water hybrid nanofluid on

✉ Pranab Kumar Mondal
pranabm@iitg.ac.in; mail2pranab@gmail.com
Sumit Kumar Mehta
sumit090391@gmail.com

¹ Department of Mechanical Engineering, National Institute of Technology Silchar, Silchar 788010, India

² Department of Mechanical Engineering, Indian Institute of Technology Guwahati, Guwahati 781039, India

natural convection inside a square cavity. It is found that the average Nusselt number enhances with volume fraction for smaller Rayleigh number, while the effect of nanoparticle volume fraction is opposite at the higher values of Rayleigh number. Sheikholeslami et al. (2019) numerically investigated the natural convective heat transfer characteristics inside a circular cavity filled with MWCNT-Fe₃O₄-water nanofluid imposing the variable magnetic forces and found that the addition of hybrid nanofluid enhances the heat transfer rate compared to the base fluid case. Moreover, a number of similar investigations have been done using the MWCNT-Fe₃O₄-water nanofluid inside porous corrugated enclosure, square porous cavity, and inverted T-shaped cavity (Izadi et al. 2018; Sajjadi et al. 2019; Mourad et al. 2021). It is found that MWCNT-Fe₃O₄-water nanofluid is a suitable hybrid nanofluid for heat transfer enhancement as the mild change in volume fraction from 0 to 0.3% augmented the thermal conductivity up to 13.89% (Sundar et al. 2014).

The use of wavy wall instead of plane wall for the heat transfer interface is one of the effective methods for heat transfer augmentation (Pati et al. 2017; Mehta and Pati 2019, 2020, 2021; Mehta et al. 2021a, 2022). Barman and Rao (2021) and Rao and Barman (2021) investigated the natural convection inside a wavy porous cavity with partial heat source. It is found that increase in amplitude and number of waves of wavy wall decreases the maximum temperature for the range of aspect ratio 0.2–5. Hamzah et al. (2021) studied the natural convection inside a porous wavy cavity filled with Al₂O₃-water nanofluid imposing a transverse magnetic source and reported that average Nusselt number decreases with amplitude of the wavy wall. Ma et al. (2020) investigated the natural convective heat transfer characteristic for the corrugated solar plant filled with Al₂O₃-water nanofluid. It is found that corrugation configuration 2 has a higher heat transfer rate among all considered configurations. Recently, a number of studies focusing on the natural convective heat transfer characteristics have been investigated using the wavy wall for the magnetohydrodynamic flow of ferrofluid, magnetohydrodynamic flow of Al₂O₃-Cu-water nanofluid, Cu-water nanofluid flow with magnetic field, and Al₂O₃-water nanofluid flow inside a crowned cavity (Ashorynejad and Shahriari 2018; Abdulkadhim et al. 2021; Afsana et al. 2021; Dogonchi et al. 2021; Hamzah et al. 2021).

We know that heat exchanging devices are associated with the loss in available energy (Kaushik et al. 2016; Gaikwad et al. 2017a; Sarma et al. 2017a). Therefore, the entropy generation should be minimum for such systems (Bhowmick et al. 2020a, b). Note that the entropy generation analysis for many thermo-fluidic devices has been done from micro to macro length scales (Chen et al. 2020; See and Leong 2020; Torabi et al. 2020; Amit et al. 2021;

Avellaneda et al. 2021; Lisboa et al. 2021; Mondal 2014; Mondal and Dholey 2015; Goswami et al. 2016; Gaikwad et al. 2017b, 2019; Mondal and Wongwises 2017, 2018; Sarma et al. 2017b, 2018, 2022; Mondal et al. 2017; Sarma and Mondal 2018; Kumar et al. 2021a, b). Afsana et al. (2021) investigated the entropy generation characteristics for MHD natural convective flow of ferrofluid inside a wavy cavity. It is found that for no-magnetic field case, the thermal and viscous entropy generation decreases with increase in nano-particle volume fraction. Dogonchi et al. (2021) studied the entropy generation characteristics for the natural convective flow inside a wavy-crowned cavity filled with Al₂O₃-water nanofluid. It is found that the increase in curvature of the cavity augmented the total entropy generation.

From an extensive review of literature, it is found that the MWCNT-Fe₃O₄-water nanofluid is suitable for heat transfer application and presence of the wavy surface enhances the heat transfer rates for natural convective flow. To the best of our knowledge, it is found that the effect of MWCNT-Fe₃O₄-water nanofluid on natural heat transfer and entropy generation characteristics inside a wavy solar plant is yet to be investigated. Considering this lacuna in the referred literature, we here consider the aforementioned aspect as the objective of the present work as discussed in detail in the subsequent sections.

2 Theoretical formulation

The simplified setup and the physical domain of wavy solar power plant based on natural convection mechanism filled with MWCNT-Fe₃O₄-water nanofluid is depicted in Fig. 1a, b, respectively. Noted that the natural convection mechanism based solar collectors are already manufactured and broadly used (Phiraphat et al. 2017; Chen and Zhang 2014). The bottom wavy wall is heated by the solar reflector and maintained at a constant temperature, T_H , and top walls are acting as cooler and temperature is maintained at T_C . The equation of the bottom wavy wall can be written as:

$$s(x) = A \sin\left(\frac{2\pi(x - 0.1L)}{L_w}\right) \quad (1)$$

Using the length scale L , the normalized form of Eq. (1) can be written as:

$$S(X) = \alpha \sin\left(\frac{2\pi(X - 0.1)}{L_w/L}\right) \quad (2)$$

Here, $S(X) = s(x)/L$, $X = x/L$, $\alpha = A/L$, and normalized wavelength, L_w/L is taken as 0.2 to generate the total number of waves equal to four.

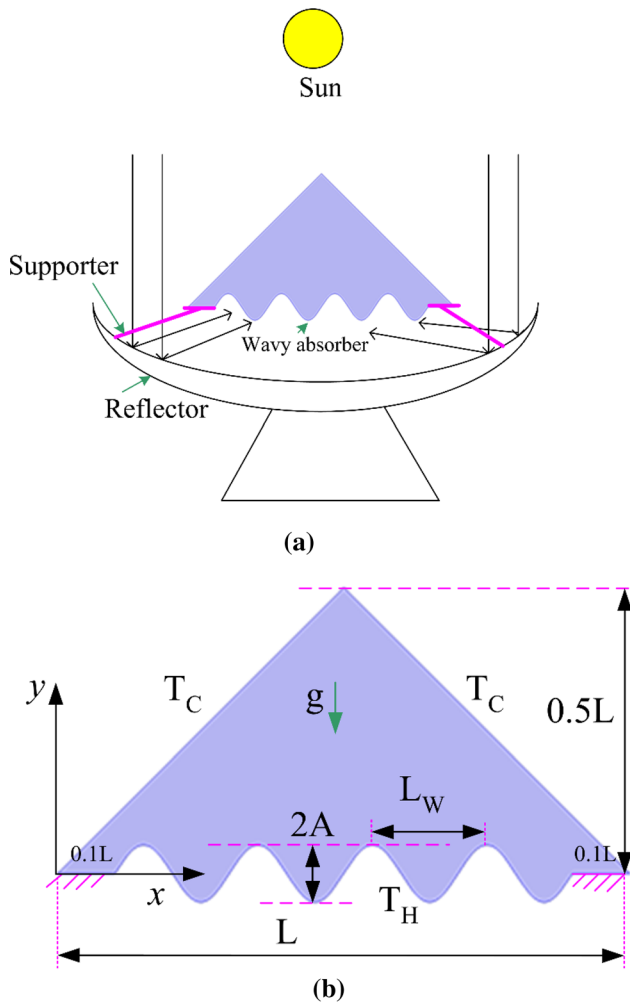


Fig. 1 a Simplified setup for solar power plant, b Computational domain of the solar power plant

We assume that the nanofluid flow through solar power plant is laminar, steady, incompressible and two-dimensional. The nanofluid distribution is considered uniform in the domain, and fluid rheology is Newtonian. Moreover, the thermo-physical properties are considered as constant except density in the body force term, where Boussinesq approximation is used. Note that the maximum temperature difference (ΔT) is achieved as ~ 7 K for the considered value of Rayleigh number ($Ra = 10^5$), $L = 0.25$ m and nanofluid volume fraction 0.3%. Following the criteria by Gray and Giorgini (1976), the Boussinesq approximation is valid when $L/\Delta T \leq 9.9 \times 10^2$ m/K for water. For the present analysis $L/\Delta T$ is obtained as 0.0357 m/K for $\Delta T = 7$ K and zero volume fraction. This order of magnitude analysis underlines for the validity of the Boussinesq approximation pertaining to this application. Further, the effects due to radiation and viscous dissipation are neglected for the chosen range of physical parameters as considered in this analysis.

Further, by using the following reference scales as $U = u/u_{ref}$, $V = v/u_{ref}$, $u_{ref} = \gamma_f/L$, $\gamma_f = k_f/(\rho_f c_{p,f})$, $\gamma_{nf} = k_{nf}/(\rho_{nf} c_{p,nf})$, $P = (pL^2)/(\rho_f \gamma_f^2)$, $Pr = \mu_f c_{p,f}/k_f$, $Ra = (\beta_f g L^3 \rho_f (T_H - T_C))/\mu_f \gamma_f$, and $\theta = (T - T_C)/(T_H - T_C)$, the dimensionless transport equations can be written as:

$$\frac{\partial U}{\partial X} + \frac{\partial V}{\partial Y} = 0 \tag{3}$$

$$\frac{\rho_{nf}}{\rho_f} \left(U \frac{\partial U}{\partial X} + V \frac{\partial U}{\partial Y} \right) = -\frac{\partial P}{\partial X} + Pr \frac{\mu_{nf}}{\mu_f} \left(\frac{\partial^2 U}{\partial X^2} + \frac{\partial^2 U}{\partial Y^2} \right) \tag{4}$$

$$\frac{\rho_{nf}}{\rho_f} \left(U \frac{\partial V}{\partial X} + V \frac{\partial V}{\partial Y} \right) = -\frac{\partial P}{\partial Y} + Pr \frac{\mu_{nf}}{\mu_f} \left(\frac{\partial^2 V}{\partial X^2} + \frac{\partial^2 V}{\partial Y^2} \right) + Ra Pr \frac{\beta_{nf}}{\beta_f} \theta \tag{5}$$

$$\left(U \frac{\partial \theta}{\partial X} + V \frac{\partial \theta}{\partial Y} \right) = \frac{\gamma_{nf}}{\gamma_f} \left(\frac{\partial^2 \theta}{\partial X^2} + \frac{\partial^2 \theta}{\partial Y^2} \right) \tag{6}$$

It is noted that the thermo-physical properties of MWCNT-Fe₃O₄-water nanofluid are taken directly from the experimentally measured value as reported in the literature and listed in Table 1 (Sundar et al. 2014). It is worth adding here that the value of thermal expansion coefficient (β) (DasGupta et al. (2014)) of MWCNT-Fe₃O₄/H₂O nanofluid is not available in the reported literature. Therefore, pertaining to the present analysis, we have used the following correlation to calculate it (Sheikholeslami et al. 2019):

$$\rho_{nf} \beta_{nf} = (1 - \phi)(\rho\beta)_f + \phi(\rho\beta)_{np} \tag{7a}$$

$$\beta_{np} = \frac{\beta_{MWCNT} \phi_{MWCNT} + \beta_{Fe_3O_4} \phi_{Fe_3O_4}}{\phi_{MWCNT} + \phi_{Fe_3O_4}} \tag{7b}$$

Here, $\beta_{Fe_3O_4}$, β_{MWCNT} and β_f are taken as $1.3 \times 10^{-5} \text{ K}^{-1}$, $4.2 \times 10^{-5} \text{ K}^{-1}$, and $2.1 \times 10^{-4} \text{ K}^{-1}$, respectively (Dutta et al. 2019; Sheikholeslami et al. 2019). The following boundary conditions are employed to solve the aforementioned transport equations:

Top wall
 $U = V = 0, \theta = 0$ (8a)

Bottom wavy wall
 $U = V = 0, \theta = 1$ (8b)

Bottom flat wall
 $U = V = 0, \partial\theta/\partial Y = 0$ (8c)

Being the dominant mode of heat transfer, the convective heat transfer rate is represented by a dimensionless number called local Nusselt number (Nu) and represented as (Dutta et al. 2019):

$$Nu = (k_{nf}/k_f)(\partial\theta/\partial N) \tag{9}$$

Table 1 Thermo-physical properties of MWCNT-Fe₃O₄-water hybrid nanofluid (Sundar et al. 2014)

ϕ (%)	Density, ρ (kg m ⁻³)	Thermal conductivity, k (Wm ⁻¹ K ⁻¹)	Dynamic viscosity, μ (mPa s)	Specific heat capacity, c_p (Jkg ⁻¹ K ⁻¹)
0	998.5	0.602	0.79	4182
0.3	1010.04	0.6856	1.01	4183.99

Here, N is the dimensionless normal along the wavy wall.

The total heat transfer rate over the heat transfer surface is represented by average Nusselt number (\overline{Nu}) and mathematically represented as (Wang and Chen 2002):

$$\overline{Nu} = \frac{\int_{X=0.1}^{X=0.9} NudS}{\int_{X=0.1}^{X=0.9} dS} \quad (10)$$

It is noted that all the fluid flow and associated transport of heat always causes destruction in available energy. Therefore, effort should be taken to keep this loss minimum to the extent possible for any heat exchanging devices/systems. Generally, the available energy loss can be represented in terms of an increase in entropy generation function. The entropy generation function pertaining to the present analysis has two components viz., thermal entropy generation and viscous entropy generation, respectively. The dimensionless form of total entropy generation (S'''_{Total}) can be written as (Dutta et al. 2019):

$$S'''_{Total} = \frac{k_{nf}}{k_f} \left(\left(\frac{\partial \theta}{\partial X} \right)^2 + \left(\frac{\partial \theta}{\partial Y} \right)^2 \right) + \phi \frac{\mu_{nf}}{\mu_f} \left(2 \left(\frac{\partial U}{\partial X} \right)^2 + 2 \left(\frac{\partial V}{\partial Y} \right)^2 + \left(\frac{\partial U}{\partial Y} + \frac{\partial V}{\partial X} \right)^2 \right) \quad (11)$$

Here, $\phi = \frac{\mu_r(T_H+T_C/2)}{k_f} (\gamma_f/L(T_H - T_C))^2$ and $S''' = (s'''L^2)/k_f$.

The averaged entropy generation in the domain can be written as (Dutta et al. 2019):

$$S_{Total} = \frac{\int S'''_{Total} d\Omega}{\int d\Omega} \quad (12)$$

Here, $d\Omega$ is the elemental area of the domain.

Now, in order to know the fractional contribution of thermal entropy generation, we define the Bejan number (Be) and given as (Dutta et al. 2019):

$$Be = \frac{S'''_{Thermal}}{S'''_{Thermal} + S'''_{Viscous}} \quad (13)$$

The average value of Bejan number in the domain can be expressed as (Dutta et al. 2019):

$$Be_{avg} = \frac{\int Be d\Omega}{\int d\Omega} \quad (14)$$

Also, we have solved the stream function to know the recirculation strength of the vortices being formed in the flow path. The dimensionless form of stream function (Ψ) can be written as:

$$\frac{\partial^2 \Psi}{\partial X^2} + \frac{\partial^2 \Psi}{\partial Y^2} = \left(\frac{\partial U}{\partial X} - \frac{\partial V}{\partial Y} \right) \quad (15)$$

Equation (15) is solved by using the computed flow field and implementing boundary condition, $\Psi = 0$ at the walls (Bhowmick et al. 2020a).

3 Numerical methodology and model benchmarking

We have solved the transport equations numerically using the commercial software COMSOL Multiphysics® v5.2 [www.comsol.com] consistent with finite element method. We here briefly discuss the numerical method employed here for the sake of completeness in the presentation. The Galerkin weighted method is implemented to convert the governing differential equations into the integral equation. First, the computational domain is sub-divided into small domain called an element. The non-uniform triangular mesh is considered, and it is denser near the walls. Further, transport variables are approximated (basis set, $\{\varphi_e\}_{e=1}^N$) using the following interpolation functions (Bhowmick et al. 2020b):

$$U = \sum_{e=1}^{N^U} \zeta_e^{U,V} U_e(X, Y), \quad V = \sum_{e=1}^{N^V} \zeta_e^{U,V} V_e(X, Y), \quad (16)$$

$$P = \sum_{e=1}^{N^P} \zeta_e^P P_e(X, Y), \quad \theta = \sum_{e=1}^{N^\theta} \zeta_e^\theta \theta_e(X, Y)$$

Here, $\zeta_e^{U,V}$, ζ_e^P and ζ_e^θ are the shape functions for velocity components, pressure and temperature, respectively, at the nodes of the element. It is noted that the “P2 + P1” type discretization is used in COMSOL Multiphysics® (Finlayson 2012), which means the quadratic shape functions are used for the velocity components and the linear shape functions are used for the pressure. Whereas the quartic shape functions are used for the

temperature. After substituting the approximated values of transport variables in the original differential equation, the residual, R is achieved, and using the method of weighted residuals, we can write:

$$\int_{\Omega} R W_e(X, Y) d\Omega = 0 \tag{17}$$

Here, $W_e(X, Y)$ is the weight function and Ω represents the domain. Therefore, the system of finite element equations are computed in close form and are non-linear in nature (Bhowmick et al. 2020b), and iteratively solved until satisfying the criteria, $|\varphi^{i+1} - \varphi^i|/\varphi^i \leq 10^{-6}$. Here, φ and i represent transport variable and integration, respectively (Mehta et al. 2021b). In addition, the grid independence test has been conducted by calculating the average Nusselt number for the different mesh types (M) as depicted in Table 2. We have selected mesh type, M3 as it gives grid unbiased result compared to the next level fine mesh type, M4.

Also, we have done extensive validation of the present numerical model essentially to establish the credibility of the proposed analysis and associated results as discussed in subsequent sections. First, as depicted in Fig. 2, the dimensionless transverse velocity component is compared with the result of Deng and Tang (2002) for natural convection inside a square cavity when Prandtl number (Pr) is 0.71 with the limiting case $\phi = 0\%$ and $\alpha = 0$. A fairly accurate match between the present and publishes results as seen in Fig. 2 justifies the accurateness of the present modeling framework. Second, the average Nusselt number at the heated wall is compared in Table 3 with the result of Deng and Tang (2002) as well as Costa (1997) for natural convection inside a square cavity, when Pr = 0.71, $\phi = 0\%$ and $\alpha = 0$. From both the comparison, we have a good match with the published works (Costa 1997; Deng and Tang 2002). Following this model benchmarking analysis, we now proceed with the discussion of the results at hand in the forthcoming sections.

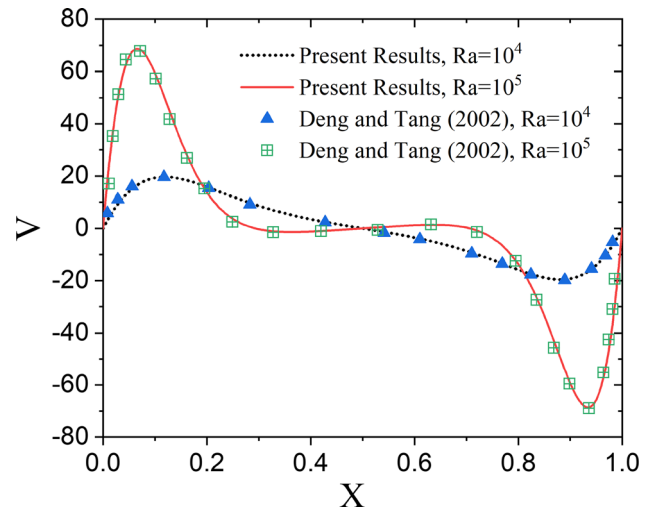


Fig. 2 Comparison of normalized y-velocity component at the horizontal line in the middle section for different Ra with the result of Deng and Tang (2002) when Pr = 0.71 and limiting case $\phi = 0\%$ and $\alpha = 0$

4 Results and discussion

In the present work, we have investigated the natural convective heat transfer and entropy generation characteristic inside a wavy solar power plant filled with MWCNT-Fe₃O₄-water nanofluid. The streamline contour, isotherm contour, local Nusselt number (Nu), average Nusselt number (\overline{Nu}), dimensionless total entropy generation (S''_{Total}), and dimensionless average total entropy generation (S_{Total}) have been studied by varying the dimensionless amplitude of the wavy wall (α) and nanoparticle volume fraction (ϕ) in the range of $0 \leq \alpha \leq 0.05$ and $0 \leq \phi \leq 0.3\%$, respectively. The value of Ra and φ are taken as 10^{-5} and 10^{-2} , respectively (Dutta et al. 2019; Sheikholeslami et al. 2019; Swain et al. 2022).

Figure 3 depicts the streamline contour for the plane and wavy solar power plant at $\phi = 0\%$ and 0.3% . It is observed that two vortices with clock-wise and contour-clock-wise circulation are generated, attributed primarily to the presence of heated wall and density difference. Further, the symmetric vortices are found for the plane wall case, while the two different vortices are predicted for the wavy wall

Table 2 Grid independency test for the different mesh system by calculating average Nusselt number (\overline{Nu}) when $\phi = 0.3\%$ and $\alpha = 0.05$

Mesh type (M)	Number of elements	Average nusselt number (\overline{Nu})	Relative error in \overline{Nu} compared to M4
M1	6166	10.742	0.500
M2	7387	10.748	0.445
M3	18,844	10.796	0
M4	24,976	10.796	0

Table 3 Comparison of average Nusselt number (\overline{Nu}) with the results of Deng and Tang (2002) and Costa (1997) when $Pr = 0.71$, and limiting case $\phi = 0\%$ and $\alpha = 0$

Deng and Tang (2002)	Costa (1997)	Present result
1.118	1.118	1.1178
2.254	2.243	2.2449
4.557	4.519	4.5219
8.826	8.8	8.8261

case. It is because of the uneven distribution of the wavy wall divided by the middle vertical section. The left side wavy wall starts with a convex surface, while the right side wavy wall ends with a concave surface. Therefore, the higher flow resistance provided by the extreme right concave wall on right side circulation causes its smaller strength. We found that the recirculation strength of vortices for wavy wall case is smaller compared to the plane wall case. It is because the flow resistance provided by the wavy wall reduces the flow strength and decreases the recirculation strength for this case as well. Furthermore, the recirculation strength for the nanofluid case ($\phi = 0.3\%$) is

smaller compared to the base fluid case ($\phi = 0\%$). This observation is attributed to the augmentation in viscosity by nanofluid compared to the base fluid case, which enhances the flow resistance and results in a reduction in the recirculation strength.

Figure 4 depicts the isotherm contours for the plane and wavy solar power plant at $\phi = 0\%$ and 0.3% . It is noted that the heating effect is higher near the wall and in the intermediate vertical region of the domain. It is attributed to the flow of hot fluid from heated wall by counter-clockwise vortex from the left side, and clockwise vortex from the right side accumulates the heated fluid in the vertical intermediate region. Further, it is noted from Fig. 4 that the heating effect in the vertical intermediate region is smaller for the case of nanofluid. We can see that the isotherm level '0.55' grown in the intermediate vertical region is smaller for $\phi = 0.3\%$ compared to $\phi = 0\%$. We attribute this observation to the stronger vortex strength for $\phi = 0\%$ (see Fig. 3) that causes transport of heated fluid up to higher vertical height in the intermediate region. Moreover, as seen in Fig. 4, the presence of wavy wall causes formation of thinner and thicker thermal boundary layer at the convex and concave surface, respectively. Important to mention,

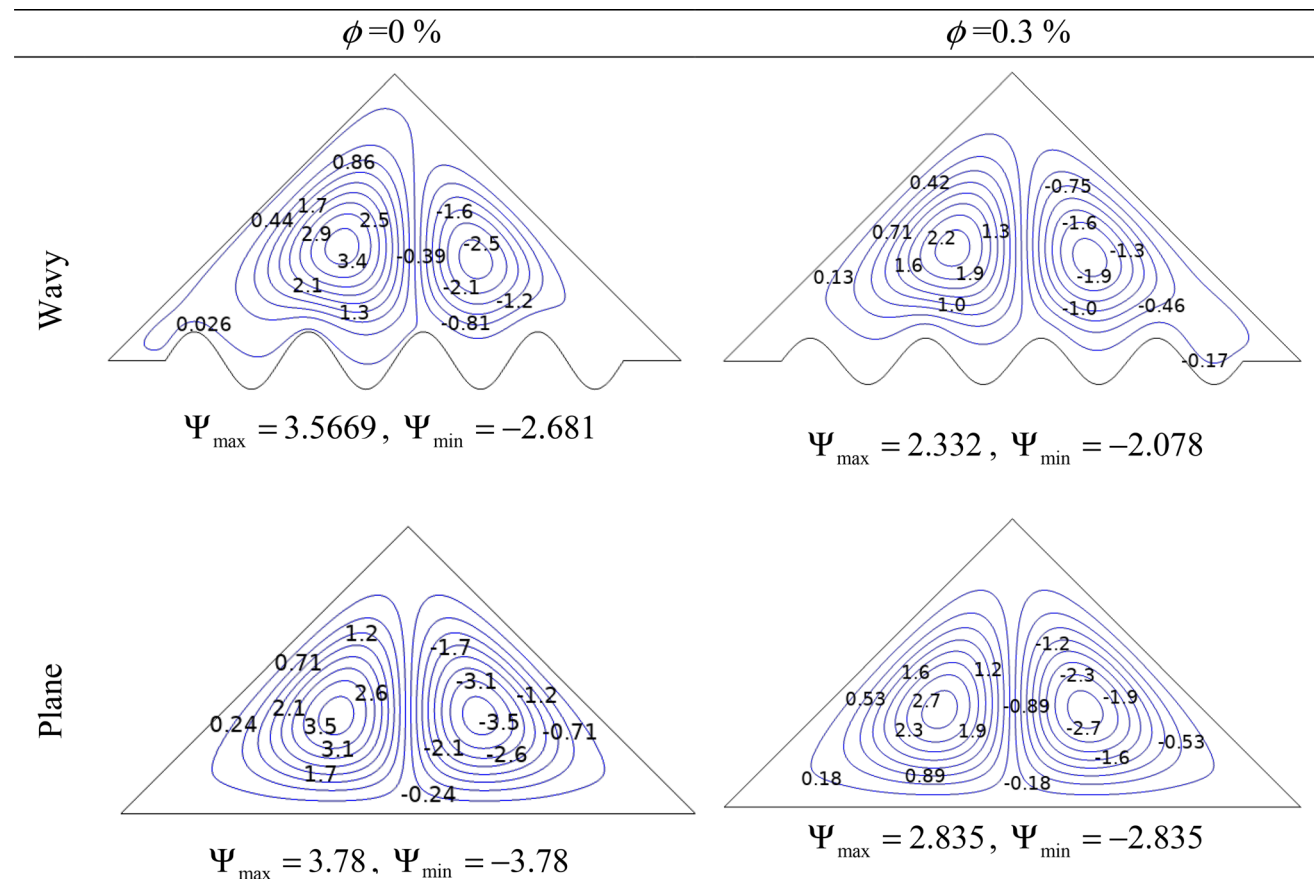


Fig. 3 Streamline contours for plane and wavy cavity ($\alpha = 0.05$) for different ϕ at $Ra = 10^5$

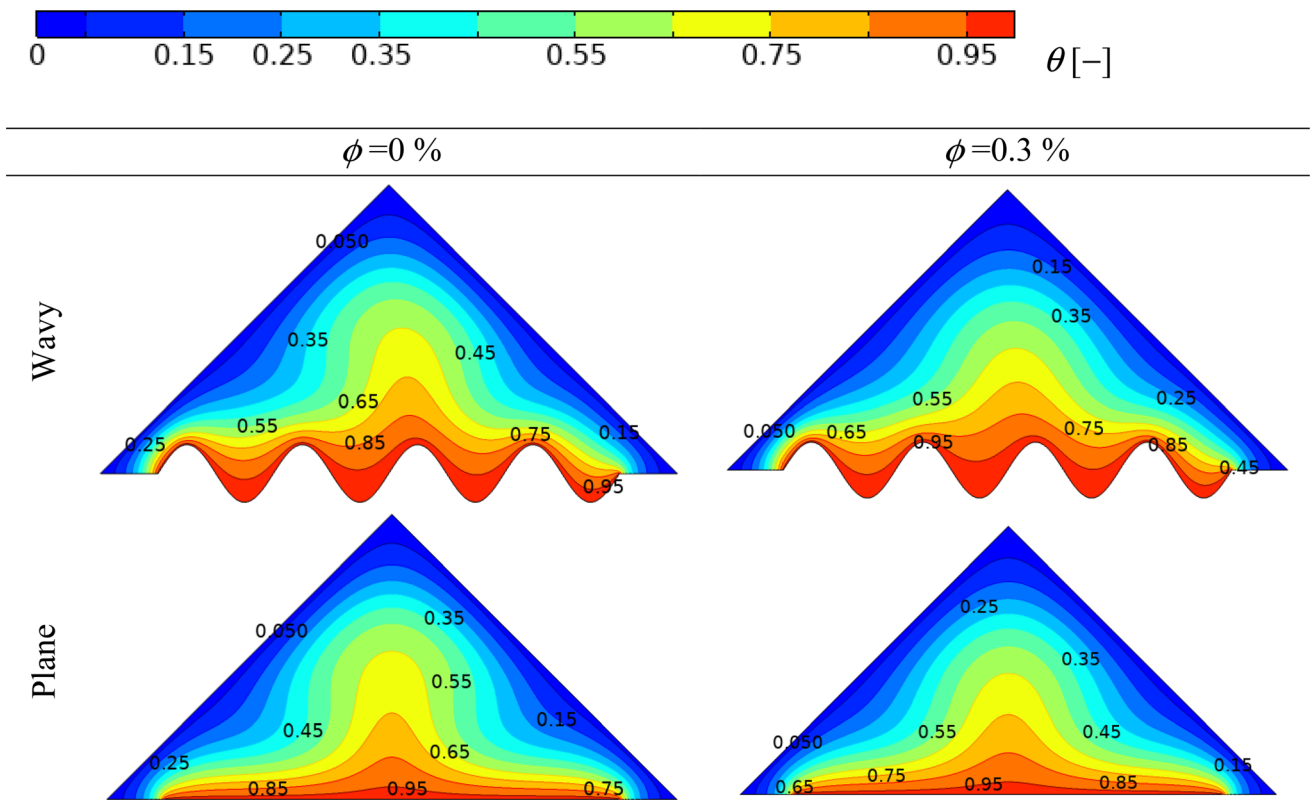


Fig. 4 Isotherm contours for plane and wavy cavity ($\alpha = 0.05$) for different ϕ at $Ra = 10^5$

the accelerated and decelerated flow rendered by the convex and concave surfaces, respectively results in such a demarcation in the configuration of the boundary layer.

Figure 5 depicts the variation of local Nusselt number (Nu) for both plane and wavy wall cases, obtained at $\phi = 0.3\%$ and $Ra = 10^5$. It is found that the local maxima and minima of Nu is predicted at the convex and concave surfaces, due to the thinner and thicker thermal boundary layer near the heated wall, respectively (see Fig. 4). We observe that the value of local maxima is smaller in the intermediate region, attributed primarily to the presence of more heated fluid in that region (see Fig. 4) reduced the heat transfer rate. It is important to mention that the all local maxima of Nu for wavy wall are higher compared to the plane wall. Contrarily, the local minima of Nu as seen for wavy wall is smaller compared to the plane wall, which is mainly due to the formation of thicker thermal boundary layer triggered by the concave wavy surface (see Fig. 4).

The overall heat transfer enhancement in wavy solar plant is represented by average Nusselt number (\overline{Nu}) and its variation with dimensionless amplitude (α) is depicted in Fig. 6. The other parameters considered are $\phi = 0$ and 0.3% when $Ra = 10^5$. It is found that the \overline{Nu} becomes higher with an increase in the amplitude of the wavy wall, signifying the combined effect of increase in heat transfer area compared to plane wall and the presence of higher

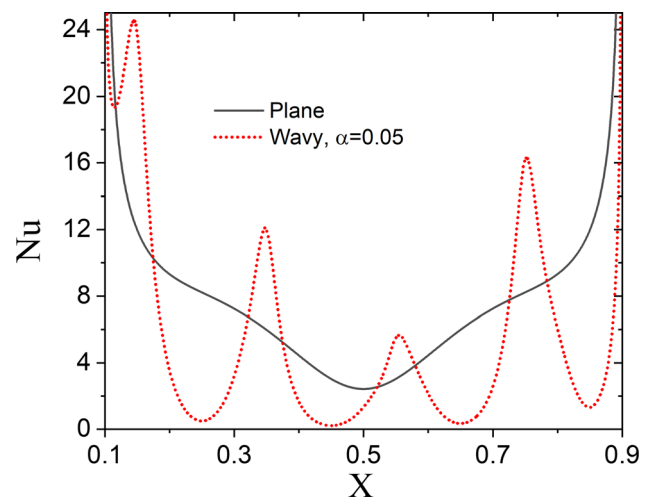


Fig. 5 Variation of local Nusselt number for plane and wavy case when $\phi = 0.3\%$ and $Ra = 10^5$

maxima of Nu at the convex region (see Fig. 5). Further, an increase in the nano-particle volume fraction from 0 to 0.3% enhances the value of \overline{Nu} . It is because of the augmentation in effective thermal conductivity of the nano-fluid compared to the base fluid case, which improves the total heat transfer rate. It is noted that the percentage enhancement in heat transfer rate are obtained as 63.52 and 66.10% for a change in $\phi = 0$ to 0.3% , respectively, with

the change in α from 0 to 0.05. On the other hand, the change in nanofluid volume fraction from 0 to 0.3% enhances the heat transfer rate up to 5.97% for $\alpha = 0.05$.

As we already know, the total entropy generation of any thermo-fluidic system should be minimum to maximize efficiency according to the second law of thermodynamics. By doing this, we can maximize the available energy of the system (Bejan 2013). Henceforward, focus is given on the entropy generation analysis as discussed in the forthcoming paragraphs. First, to know the fractional contribution of thermal entropy generation on the total entropy generation (thermal and viscous) in the domain, the variation of average Bejan number (Be_{avg}) is depicted in Fig. 7. The plots are obtained for α , $\phi = 0, 0.3\%$ and $Ra = 10^5$. It is found from Fig. 7 that $Be_{avg} \ll 0.5$ for all the values of ϕ considered. This observation signifies that the entropy generation due to viscous dissipation is dominating over the thermal entropy generation in the domain. It may be mentioned here that the higher value of $Ra (= 10^5)$ leads to the development of stronger flow field and resulting in higher contribution of viscous dissipation dominated entropy generation (Dutta et al. 2019). We find that the value of Be_{avg} enhances with an increase in the wave amplitude. It is based on the fact that the contribution of viscous entropy generation reduces with an increase in amplitude and is explained as follows. The increase in the sharpness of diverging wavy surface with an increase in amplitude decreases the flow field strength to satisfy the mass conservation in the field, and it reduces the velocity gradient with amplitude. Therefore, the reduction in velocity gradient and accordingly viscous entropy generation with an increase in amplitude near the diverging walls increases the value of Be_{avg} . Moreover, the value of Be_{avg}

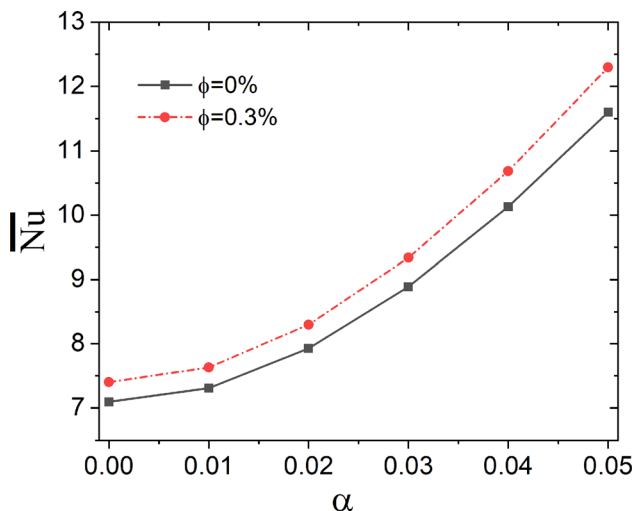


Fig. 6 Variation of average Nusselt number with dimensionless amplitude for wavy case at $\phi = 0$ and 0.3% when $Ra = 10^5$

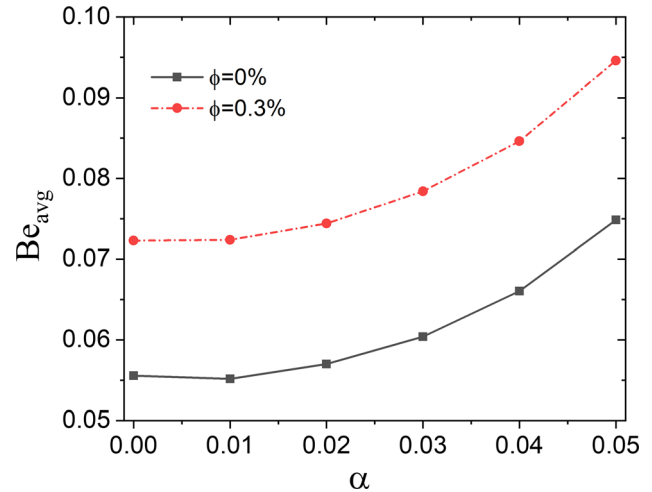


Fig. 7 Variation of average Bejan number with dimensionless amplitude for wavy case at $\phi = 0$ and 0.3% when $Ra = 10^5$

enhances with ϕ . It is due to the fact that a decrease in recirculation strength for the nanofluid case as compared to the base fluid case (see Fig. 3) leads to a decrease in the velocity gradient at the interfaces of two opposite streams of the flow (clock-wise and counter-clock-wise) and near the wall with ϕ . Therefore, a decrease in entropy generation due to viscous dissipation for the nanofluid case leads to an increase in the value of Be_{avg} with ϕ as witnessed in Fig. 7.

Figure 8 depicts the contour of the dimensionless total entropy generation (S''_{Total}) for both the plane and wavy solar power plant, obtained at $\phi = 0$ and 0.3%. The distribution of S''_{Total} can be explained from the variation of velocity gradient in the domain as the entropy generation due to viscous dissipation is dominating one (see Fig. 7). It is noted that the intensity of S''_{Total} is higher at the attachment region of vortices, i.e., at the top and bottom walls and in the region of attachment and detachment of two vortices. The combined effects like the generation of higher velocity gradient near the walls and the interaction of two opposite stream of vortices at the attachment and detachment region give rise to higher viscous entropy generation and S''_{Total} . Further, the presence of wavy wall decreases the intensity of S''_{Total} near the bottom wall. It is attributed to the presence of concave surface that decreases the velocity gradient and results in a decrease of the viscous dissipation modulated entropy generation compared to the plane wall. Also, the decrease in recirculation strength with ϕ decreases the viscous dissipation modulated entropy generation and the intensity of S''_{Total} .

The overall entropy generation in domain represented by dimensionless averaged total entropy generation (S_{Total}) and corresponding variation with dimensionless amplitude (α) is depicted in Fig. 9. The other parameters chosen for

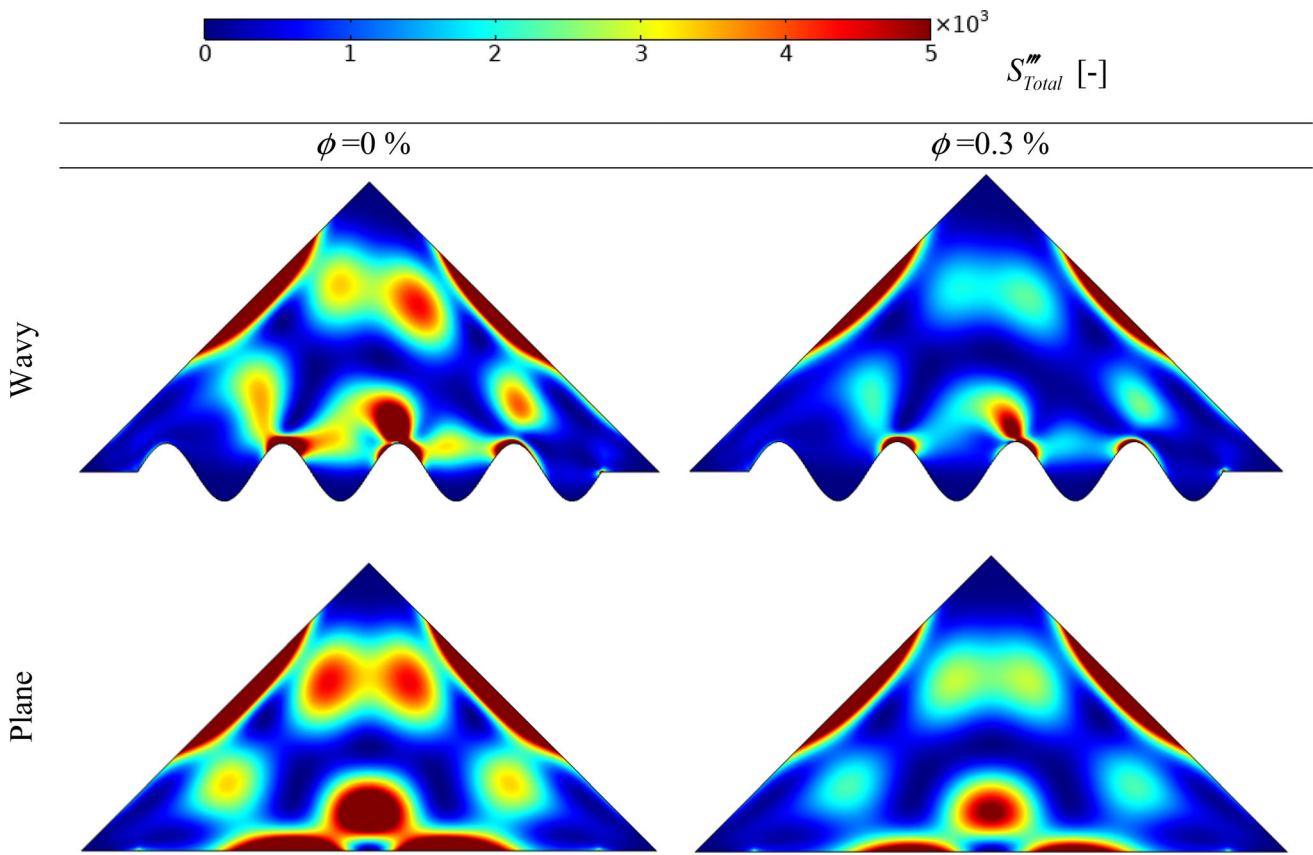


Fig. 8 Dimensionless total entropy generation contours for plane and wavy cavity ($\alpha = 0.05$) for different ϕ at $Ra = 10^5$

plotting the figure are $\phi = 0$ and 0.3% , $Ra = 10^5$. It is noted that the value of S_{Total} decreases with α and ϕ , attributed primarily to the decrease in total entropy generation intensity by the wavy wall compared to the plane wall and the decrease in the same by nanofluid compared to the base fluid case (see Fig. 8). It is noted that the percentage decrement in S_{Total} are obtained as 23.03% and 29.77% for $\phi = 0$ to 0.3% , respectively, with the change in α from 0 to 0.05. On the other hand, the change in nanofluid volume fraction from 0 to 0.3% enhances the heat transfer rate up to 40.01% for $\alpha = 0.05$.

5 Conclusion

We have investigated the natural convective heat transfer and entropy generation characteristic inside a wavy solar power plant filled with MWCNT-Fe₃O₄-water nanofluid numerically consistent with the finite element method. The streamline contour, isotherm contour, local Nusselt number (Nu), average Nusselt number (\overline{Nu}), dimensionless total entropy generation (S''_{Total}), and dimensionless average total entropy generation (S_{Total}) have been studied by varying the dimensionless amplitude of the wavy wall (α)

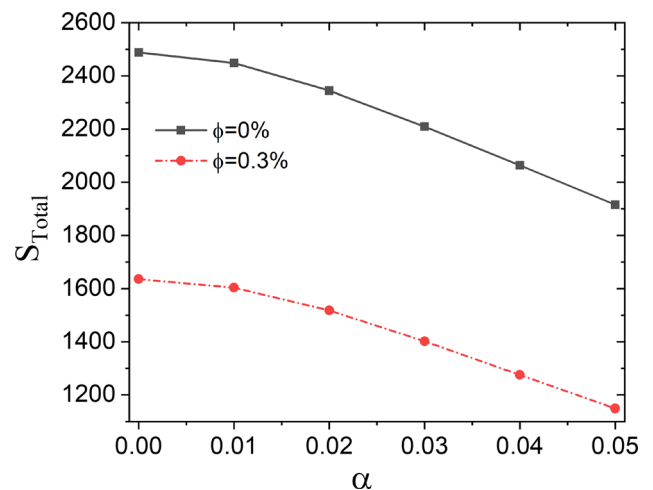


Fig. 9 Variation of average dimensionless total entropy generation with dimensionless amplitude for wavy case at $\phi = 0$ and 0.3% when $Ra = 10^5$

and nano-particle volume fraction (ϕ). It is found that the presence of wavy wall and addition of nano-particle in base fluid decreases the recirculation strength appreciably. The increase in amplitude of wavy wall and nano-particle volume fraction enhances the average Nusselt number

significantly. Moreover, the viscous entropy generation is seen to be the dominating mode towards bringing irreversibility into the system for the chosen value of Ra. The increase in wave amplitude and nano-particle volume fraction reduces the average entropy generation. We found 40.01% reduction in average value of total entropy generation rate for a change in nano-particle volume fraction from 0 to 0.3% when $\alpha = 0.05$. The findings from the present work are found to be of importance in designing an efficient solar power plant.

References

- Abdulkadhim A, Hamzah HK, Ali FH et al (2021) Effect of heat generation and heat absorption on natural convection of Cu-water nanofluid in a wavy enclosure under magnetic field. *Int Commun Heat Mass Transf*. <https://doi.org/10.1016/j.icheatmasstransfer.2020.105024>
- Afsana S, Molla MM, Nag P et al (2021) MHD natural convection and entropy generation of non-newtonian ferrofluid in a wavy enclosure. *Int J Mech Sci* 198:106350. <https://doi.org/10.1016/j.ijmeosci.2021.106350>
- Alblawi A, Zainuddin N, Roslan R et al (2020) Effect of heat generation on mixed convection in porous cavity with sinusoidal heated moving lid and uniformly heated or cooled bottom walls. *Microsyst Technol* 26:1531–1542. <https://doi.org/10.1007/s00542-019-04690-y>
- Amit K, Datta A, Biswas N et al (2021) Designing of microsink to maximize the thermal performance and minimize the entropy generation with the role of flow structures. *Int J Heat Mass Transf* 176:121421. <https://doi.org/10.1016/j.ijheatmasstransfer.2021.121421>
- Ashorynejad HR, Shahriari A (2018) MHD natural convection of hybrid nanofluid in an open wavy cavity. *Results Phys* 9:440–455. <https://doi.org/10.1016/j.rinp.2018.02.045>
- Avellaneda JM, Bataille F, Toutant A, Flamant G (2021) DNS Of entropy generation rates for turbulent flows subjected to high temperature gradients. *Int J Heat Mass Transf* 176:121463. <https://doi.org/10.1016/j.ijheatmasstransfer.2021.121463>
- Barman P, Rao PS (2021) Effect of aspect ratio on natural convection in a wavy porous cavity submitted to a partial heat source. *Int Commun Heat Mass Transf* 126:105453. <https://doi.org/10.1016/j.icheatmasstransfer.2021.105453>
- Bejan A (2013) *Convection heat transfer*, 4th edn. Wiley, Hoboken, New Jersey. <https://doi.org/10.1002/9781118671627.ch12>
- Bhowmick D, Chakravarthy S, Randive PR, Pati S (2020a) Numerical investigation on the effect of magnetic field on natural convection heat transfer from a pair of embedded cylinders within a porous enclosure. *J Therm Anal Calorim* 141:2405–2427. <https://doi.org/10.1007/s10973-020-09411-6>
- Bhowmick D, Randive PR, Pati S et al (2020b) Natural convection heat transfer and entropy generation from a heated cylinder of different geometry in an enclosure with non-uniform temperature distribution on the walls. *J Therm Anal Calorim* 141:839–857. <https://doi.org/10.1007/s10973-019-09054-2>
- Brusly Solomon A, Sharifpur M, Ottermann T et al (2017a) Natural convection enhancement in a porous cavity with Al₂O₃-ethylene glycol/water nanofluids. *Int J Heat Mass Transf* 108:1324–1334. <https://doi.org/10.1016/j.ijheatmasstransfer.2017.01.009>
- Brusly Solomon A, van Rooyen J, Rencken M et al (2017b) Experimental study on the influence of the aspect ratio of square cavity on natural convection heat transfer with Al₂O₃/water nanofluids. *Int Commun Heat Mass Transf* 88:254–261. <https://doi.org/10.1016/j.icheatmasstransfer.2017.09.007>
- Chen L, Zhang XR (2014) Experimental analysis on a novel solar collector system achieved by supercritical CO₂ natural convection. *Energy Convers Manage* 77:173–182. <https://doi.org/10.1016/j.enconman.2013.08.059>
- Chen J, Han D, He W (2020) Thermodynamic balancing of heat and mass transfer process to minimize its entropy generation by mass injection and extraction. *Int J Heat Mass Transf* 161:120261. <https://doi.org/10.1016/j.ijheatmasstransfer.2020.120261>
- COMSOL multiphysics® v. 5.2 (2015). www.comsol.com. COMSOL AB, Stockholm, Sweden. Accessed 1 Oct 2021
- Costa VAF (1997) Double diffusive natural convection in a square enclosure with heat and mass diffusive walls. *Int J Heat Mass Transf* 40:4061–4071. [https://doi.org/10.1016/S0017-9310\(97\)00061-6](https://doi.org/10.1016/S0017-9310(97)00061-6)
- DasGupta D, Mondal PK, Chalraborty S (2014) Thermocapillary-actuated contact-line motion of immiscible binary fluids over substrates with patterned wettability in narrow confinement. *Phys Rev E* 90(2):023011. <https://doi.org/10.1103/PhysRevE.90.023011>
- Deng Q-H, Tang G-F (2002) Numerical visualization of mass and heat transport for conjugate natural convection/heat conduction by streamline and headline. *Int J Heat Mass Transf* 45:2373–2385. [https://doi.org/10.1016/S0017-9310\(01\)00316-7](https://doi.org/10.1016/S0017-9310(01)00316-7)
- Dogonchi AS, Sadeghi MS, Ghodrati M et al (2021) Natural convection and entropy generation of a nanofluid in a crown wavy cavity: effect of thermo-physical parameters and cavity shape. *Case Stud Therm Eng* 27:101208. <https://doi.org/10.1016/j.csite.2021.101208>
- Dutta S, Goswami N, Biswas AK, Pati S (2019) Numerical investigation of magnetohydrodynamic natural convection heat transfer and entropy generation in a rhombic enclosure filled with Cu-water nanofluid. *Int J Heat Mass Transf* 136:777–798. <https://doi.org/10.1016/j.ijheatmasstransfer.2019.03.024>
- Ebrahimpour Z, Farshad SA, Sheikholeslami M (2021) Nanofluid migration within an absorber pipe of solar unit considering radiation mechanism. *Microsyst Technol* 27:2117–2130. <https://doi.org/10.1007/s00542-020-05113-z>
- Farshad SA, Sheikholeslami M, Hosseini SH et al (2019) Nanofluid turbulent forced convection through a solar flat plate collector with Al₂O₃ nanoparticles. *Microsyst Technol* 25:4237–4247. <https://doi.org/10.1007/s00542-019-04430-2>
- Finlayson BA (2012) Appendix D: Hints when using comsol multiphysics®. In: Finlayson BA (Ed). *Introduction to chemical engineering computing*. <https://doi.org/10.1002/9781118309599.app4>
- Gaikwad HS, Mondal PK, Wongwises S (2017a) Non-linear drag induced entropy generation analysis in a microporous channel: the effect of conjugate heat transfer. *Int J Heat Mass Transf* 108:2217–2228. <https://doi.org/10.1016/j.ijheatmasstransfer.2017.01.041>
- Gaikwad HS, Basu DN, Mondal PK (2017b) Non-linear drag induced irreversibility minimization in a viscous dissipative flow through a micro-porous channel. *Energy* 119:588–600. <https://doi.org/10.1016/j.energy.2016.11.020>
- Gaikwad HS, Roy A, Mondal PK et al (2019) Irreversibility analysis in a slip aided electroosmotic flow through an asymmetrically heated microchannel: The effects of joule heating and the conjugate heat transfer. *Anal Chim Acta* 1045:85–97. <https://doi.org/10.1016/j.aca.2018.08.058>
- Ghalambaz M, Doostani A, Izadpanahi E, Chamkha AJ (2020) Conjugate natural convection flow of Ag–MgO/water hybrid

- nanofluid in a square cavity. *J Therm Anal Calorim* 139:2321–2336. <https://doi.org/10.1007/s10973-019-08617-7>
- Goswami P, Mondal PK, Datta A, Chakraborty S (2016) Entropy generation minimization in an electroosmotic flow of non-newtonian fluid: effect of conjugate heat transfer. *J Heat Transfer* 138(5):051704. <https://doi.org/10.1115/1.4032431>
- Goudarzi S, Shekaramiz M, Omidvar A et al (2020) Nanoparticles migration due to thermophoresis and brownian motion and its impact on Ag-MgO/Water hybrid nanofluid natural convection. *Powder Technol* 375:493–503. <https://doi.org/10.1016/j.powtec.2020.07.115>
- Gray DD, Giorgini A (1976) The validity of the boussinesq approximation for liquids and gases. *Int J Heat Mass Transf* 19(5):545–551. [https://doi.org/10.1016/0017-9310\(76\)90168-X](https://doi.org/10.1016/0017-9310(76)90168-X)
- Hamzah H, Albojamal A, Sahin B, Vafai K (2021) Thermal management of transverse magnetic source effects on nanofluid natural convection in a wavy porous enclosure. *J Therm Anal Calorim* 143:2851–2865. <https://doi.org/10.1007/s10973-020-10246-4>
- Huang YC, Hsu HC (2019) Numerical simulation and experimental validation of heat sinks fabricated using selective laser melting for use in a compact LED recessed downlight. *Microsyst Technol* 25:121–137. <https://doi.org/10.1007/s00542-018-3943-x>
- Izadi M, Mohebbi R, Karimi D, Sheremet MA (2018) Numerical simulation of natural convection heat transfer inside a T shaped cavity filled by a MWCNT-Fe₃O₄/water hybrid nanofluids using LBM. *Chem Eng Process—Process Intensif* 125:56–66. <https://doi.org/10.1016/j.cep.2018.01.004>
- Izadi M, Mohebbi R, Delouei AA, Sajjadi H (2019) Natural convection of a magnetizable hybrid nanofluid inside a porous enclosure subjected to two variable magnetic fields. *Int J Mech Sci* 151:154–169. <https://doi.org/10.1016/j.ijmecsci.2018.11.019>
- Kaushik P, Mondal PK, Pati S, Chakraborty S (2016) Heat transfer and entropy generation characteristics of a non-newtonian fluid squeezed and extruded between two parallel plates. *J Heat Transf*. <https://doi.org/10.1115/1.4034898>
- Krishna CM, ViswanathaReddy G, Souayah B et al (2019) Thermal convection of MHD Blasius and Sakiadis flow with thermal convective conditions and variable properties. *Microsyst Technol* 25:3735–3746. <https://doi.org/10.1007/s00542-019-04353-y>
- Kumar K, Kumar R, Bharj RS, Mondal PK (2021a) Irreversibility analysis of the convective flow through corrugated channels: a comprehensive review. *Eur Phys J plus* 136:402. <https://doi.org/10.1140/epjp/s13360-021-01388-x>
- Kumar KG, Hani EHB, Assad MEH et al (2021b) A novel approach for investigation of heat transfer enhancement with ferromagnetic hybrid nanofluid by considering solar radiation. *Microsyst Technol* 27:97–104. <https://doi.org/10.1007/s00542-020-04920-8>
- Kumar M, Mondal PK (2022) Irreversibility analysis of hybrid nanofluid flow over a rotating disk: effect of thermal radiation and magnetic field. *Coll Surf A Physicochem Eng Asp* 635:128077. <https://doi.org/10.1016/j.colsurfa.2021.128077>
- Lisboa KM, Zotin JLZ, Naveira-Cotta CP, Cotta RM (2021) Leveraging the entropy generation minimization and designed porous media for the optimization of heat sinks employed in low-grade waste heat harvesting. *Int J Heat Mass Transf* 181:121850. <https://doi.org/10.1016/j.ijheatmasstransfer.2021.121850>
- Ma Y, Rashidi MM, Mohebbi R, Yang Z (2020) Nanofluid natural convection in a corrugated solar power plant using the hybrid LBM-TVD method. *Energy* 199:117402. <https://doi.org/10.1016/j.energy.2020.117402>
- Mansour MA, Siddiqa S, Gorla RSR, Rashad AM (2018) Effects of heat source and sink on entropy generation and MHD natural convection of Al₂O₃-Cu/water hybrid nanofluid filled with square porous cavity. *Therm Sci Eng Prog* 6:57–71. <https://doi.org/10.1016/j.tsep.2017.10.014>
- Mehta SK, Pati S (2019) Analysis of thermo-hydraulic performance and entropy generation characteristics for laminar flow through triangular corrugated channel. *J Therm Anal Calorim* 136:49–62. <https://doi.org/10.1007/s10973-018-7969-1>
- Mehta SK, Pati S (2020) Numerical study of thermo-hydraulic characteristics for forced convective flow through wavy channel at different prandtl numbers. *J Therm Anal Calorim* 141:2429–2451. <https://doi.org/10.1007/s10973-020-09412-5>
- Mehta SK, Pati S (2021) Thermo-hydraulic and entropy generation analysis for magnetohydrodynamic pressure driven flow of nanofluid through an asymmetric wavy channel. *Int J Numer Methods Heat Fluid Flow* 31:1190–1213. <https://doi.org/10.1108/HFF-05-2020-0300>
- Mehta SK, Pati S, Ahmed S et al (2021a) Analysis of thermo-hydraulic and entropy generation characteristics for flow through ribbed-wavy channel. *Int J Numer Methods Heat Fluid Flow*. <https://doi.org/10.1108/HFF-01-2021-0056>
- Mehta SK, Pati S, Mondal PK (2021b) Numerical study of the vortex-induced electroosmotic mixing of non-newtonian biofluids in a nonuniformly charged wavy microchannel: effect of finite ion size. *Electrophoresis* 42:2498–2510. <https://doi.org/10.1002/elps.202000225>
- Mehta SK, Pati S, Baranyi L (2022) Effect of amplitude of walls on thermal and hydrodynamic characteristics of laminar flow through an asymmetric wavy channel. *Case Stud Therm Eng* 31:101796. <https://doi.org/10.1016/j.csite.2022.101796>
- Mondal PK (2014) Entropy analysis for the Couette flow of non-newtonian fluids between asymmetrically heated parallel plates: effect of applied pressure gradient. *Phys Scr* 89:125003. <https://doi.org/10.1088/0031-8949/89/12/125003>
- Mondal PK, Dholey S (2015) Effect of conjugate heat transfer on the irreversibility generation rate in a combined couette-poiseuille flow between asymmetrically heated parallel plates: the entropy minimization analysis. *Energy* 83:55–64. <https://doi.org/10.1016/j.energy.2015.01.078>
- Mondal PK, Wongwises S (2017) Irreversibility analysis in a low peclet-number electroosmotic transport through an asymmetrically heated microchannel. *Int J Exergy* 22:29–53. <https://doi.org/10.1504/IJEX.2017.081200>
- Mondal PK, Wongwises S (2018) Assessment of thermodynamic irreversibility in a micro-scale viscous dissipative circular couette flow. *Entropy* 20(1):50. <https://doi.org/10.3390/e20010050>
- Mondal PK, Wongwises S (2020) Magneto-hydrodynamic (MHD) micropump of nanofluids in a rotating microchannel under electrical double-layer effect. *Proc Inst Mech Eng Part E J Process Mech Eng* 234:318–330. <https://doi.org/10.1177/0954408920921697>
- Mondal PK, Gaikwad H, Kundu PK, Wongwises S (2017) Effect of thermal asymmetries on the entropy generation analysis of a variable viscosity couette-poiseuille flow. *Proc Inst Mech Eng Part E J Process Mech Eng* 231:1011–1024. <https://doi.org/10.1177/0954408916688234>
- Mourad A, Aissa A, Mebarek-Oudina F et al (2021) Galerkin finite element analysis of thermal aspects of Fe₃O₄-MWCNT/water hybrid nanofluid filled in wavy enclosure with uniform magnetic field effect. *Int Commun Heat Mass Transf* 126:105461. <https://doi.org/10.1016/j.icheatmasstransfer.2021.105461>
- Pati S, Mehta SK, Borah A (2017) Numerical investigation of thermo-hydraulic transport characteristics in wavy channels: comparison between raccoon and serpentine channels. *Int Commun Heat Mass Transf* 88:171–176. <https://doi.org/10.1016/j.icheatmasstransfer.2017.09.001>

- Phiraphat S, Prommas R, Puangsombut W (2017) Experimental study of natural convection in PV roof solar collector. *Int Commun Heat Mass Transf* 89:31–38. <https://doi.org/10.1016/j.icheatmasstransfer.2017.09.022>
- Rao PS, Barman P (2021) Natural convection in a wavy porous cavity subjected to a partial heat source. *Int Commun Heat Mass Transf* 120:105007. <https://doi.org/10.1016/j.icheatmasstransfer.2020.105007>
- Roy NC (2022) MHD natural convection of a hybrid nanofluid in an enclosure with multiple heat sources. *Alexandria Eng J* 61:1679–1694. <https://doi.org/10.1016/j.aej.2021.06.076>
- Sajjadi H, Amiri Delouei A, Izadi M, Mohebbi R (2019) Investigation of MHD natural convection in a porous media by double MRT lattice Boltzmann method utilizing MWCNT–Fe₃O₄/water hybrid nanofluid. *Int J Heat Mass Transf* 132:1087–1104. <https://doi.org/10.1016/j.ijheatmasstransfer.2018.12.060>
- Sarma R, Mondal PK (2018) Entropy generation minimization in a pressure-driven microflow of viscoelastic fluid with slippage at the wall: effect of conjugate heat transfer. *J Heat Transf* 140(5):052402. <https://doi.org/10.1115/1.4038451>
- Sarma R, Jain M, Mondal PK (2017a) Towards the minimization of thermodynamic irreversibility in an electrically actuated microflow of a viscoelastic fluid under electrical double layer phenomenon. *Phys Fluids* 29:103102. <https://doi.org/10.1063/1.4991597>
- Sarma R, Gaikwad H, Mondal PK (2017b) Effect of conjugate heat transfer on entropy generation in slip-driven microflow of power law fluids. *Nanoscale Microscale Thermophys Eng* 21:26–44. <https://doi.org/10.1080/15567265.2016.1272655>
- Sarma R, Nath AJ, Konwar T et al (2018) Thermo-hydrodynamics of a viscoelastic fluid under asymmetrical heating. *Int J Heat Mass Transf* 125:515–524. <https://doi.org/10.1016/j.ijheatmasstransfer.2018.04.013>
- Sarma R, Shukla AK, Gaikwad HS et al (2022) Effect of conjugate heat transfer on the thermo-electro-hydrodynamics of nanofluids: entropy optimization analysis. *J Therm Anal Calorim* 147:599–614. <https://doi.org/10.1007/s10973-020-10341-6>
- See YS, Leong KC (2020) Entropy generation for flow boiling on a single semi-circular minichannel. *Int J Heat Mass Transf* 154:119689. <https://doi.org/10.1016/j.ijheatmasstransfer.2020.119689>
- Selimefendigil F, Oztop HF (2019) Mixed convection and entropy generation of nanofluid flow in a vented cavity under the influence of inclined magnetic field. *Microsyst Technol* 25:4427–4438. <https://doi.org/10.1007/s00542-019-04350-1>
- Sheikholeslami M, Mehryan SAM, Shafee A, Sheremet MA (2019) Variable magnetic forces impact on magnetizable hybrid nanofluid heat transfer through a circular cavity. *J Mol Liq* 277:388–396. <https://doi.org/10.1016/j.molliq.2018.12.104>
- Shyam S, Yadav A, Gawade Y et al (2020) Dynamics of a single isolated ferrofluid plug inside a micro-capillary in the presence of externally applied magnetic field. *Exp Fluids* 61:210. <https://doi.org/10.1007/s00348-020-03043-0>
- Shyam S, Mondal PK, Mehta B (2021) Magneto-fluidic mixing of a ferrofluid droplet under the influence of a time-dependent external field. *J Fluid Mech*. <https://doi.org/10.1017/jfm.2021.245>
- Sundar LS, Singh MK, Sousa ACM (2014) Enhanced heat transfer and friction factor of MWCNT–Fe₃O₄/water hybrid nanofluids. *Int Commun Heat Mass Transf* 52:73–83. <https://doi.org/10.1016/j.icheatmasstransfer.2014.01.012>
- Sureshkumar Raju S, Ganesh Kumar K, Rahimi-Gorji M, Khan I (2019) Darcy-Forchheimer flow and heat transfer augmentation of a viscoelastic fluid over an incessant moving needle in the presence of viscous dissipation. *Microsyst Technol* 25:3399–3405. <https://doi.org/10.1007/s00542-019-04340-3>
- Swain K, Mebarek-Oudina F, Abo-Dahab SM (2022) Influence of MWCNT/Fe₃O₄ hybrid nanoparticles on an exponentially porous shrinking sheet with chemical reaction and slip boundary conditions. *J Therm Anal Calorim*. 147:1561–1570. <https://doi.org/10.1007/s10973-020-10432-4>
- Tayebi T, Chamkha AJ (2021) Effects of various configurations of an inserted corrugated conductive cylinder on MHD natural convection in a hybrid nanofluid-filled square domain. *J Therm Anal Calorim* 143:1399–1411. <https://doi.org/10.1007/s10973-020-10206-y>
- Torabi M, Karimi N, Torabi M et al (2020) Generation of entropy in micro thermofluidic and thermochemical energy systems—a critical review. *Int J Heat Mass Transf* 163:120471. <https://doi.org/10.1016/j.ijheatmasstransfer.2020.120471>
- Tyagi PK, Kumar R, Mondal PK (2020) A review of the state-of-the-art nanofluid spray and jet impingement cooling. *Phys Fluids* 32:121301. <https://doi.org/10.1063/5.0033503>
- Wang CC, Chen CK (2002) Forced convection in a wavy-wall channel. *Int J Heat Mass Transf* 45:2587–2595. [https://doi.org/10.1016/S0017-9310\(01\)00335-0](https://doi.org/10.1016/S0017-9310(01)00335-0)

Publisher's Note Springer Nature remains neutral with regard to jurisdictional claims in published maps and institutional affiliations.